

## Effects of unloading by tail suspension on biological apatite crystallite alignment in mouse femur

Kosuke NAKAJIMA<sup>1,2</sup>, Satoru MATSUNAGA<sup>2,3</sup>, Toshiyuki MORIOKA<sup>2,4</sup>, Takayoshi NAKANO<sup>5</sup>, Shinichi ABE<sup>2,3</sup>, Yoshitaka FURUYA<sup>1,2</sup> and Yasutomo YAJIMA<sup>1,2</sup>

<sup>1</sup> Department of Oral and Maxillofacial Implantology, Tokyo Dental College, 2-9-18 Misaki-cho, Chiyoda-ku, Tokyo 101-0061, Japan

<sup>2</sup> Oral Health Science Center, Tokyo Dental College, 2-9-18 Misaki-cho, Chiyoda-ku, Tokyo 101-0061, Japan

<sup>3</sup> Department of Anatomy, Tokyo Dental College, 2-9-18 Misaki-cho, Chiyoda-ku, Tokyo 101-0061, Japan

<sup>4</sup> Department of Removable Partial Prosthodontics, Tokyo Dental College, 2-9-18 Misaki-cho, Chiyoda-ku, Tokyo 101-0061, Japan

<sup>5</sup> Division of Materials and Manufacturing Science, Graduate School of Engineering, Osaka University, 2-1 Yamadaoka, Suita-shi, Osaka 565-0871, Japan

Corresponding author, Satoru MATSUNAGA; E-mail: matsuna@tdc.ac.jp

The aim of this study was clarify the effects of reducing various functional pressures essential for the maintenance of bone homeostasis. Femoral bone mineral density (BMD) and biological apatite (BAP) crystallite alignment were measured in conventionally reared and hindlimb-unloaded mice. The femur was divided into 10 equal segments perpendicular to the longitudinal axis of the bone and measurements were performed on the cortical bone in the five segments closest to the midpoint of the femur. Significantly lower BMD and BAP alignment in the longitudinal (Z-axis) direction were observed in the hindlimb-unloaded group. The present findings suggest that unloading by tail suspension significantly decreases not only mouse femoral bone mass but also BAP crystallite alignment, although minimal uniaxial preferential alignment is retained.

**Keywords:** Hindlimb-unloading, Femur, Bone quality, Biological apatite crystallite alignment, Bone mineral density (BMD)

### INTRODUCTION

Bone mass and strength decrease during spaceflight and prolonged immobility in the elderly due to reductions in the functional pressures exerted by forces such as gravity and exercise<sup>1-4</sup>. Mechanical stress is essential for the maintenance of bone mass and morphology<sup>5,6</sup>. In his mechanostat theory, Frost postulated that bone formation is promoted by moderate loading, while bone resorption is promoted by reduced loading<sup>7</sup>. Rodan *et al.* support the validity of this theory, reporting the importance of an appropriate load environment for maintaining bone structure<sup>8,9</sup>. However, in addition to the weight of the bone itself, muscle and various other functional pressures are exerted on the bone, resulting in a complex load-transfer path<sup>10</sup>. Functional pressure varies between bones and it is extremely difficult to analyze the strength of each bone individually. In *in vivo* studies, it is possible to measure applied external forces at the macroscopic level, but it is difficult to calculate strain at the microscopic level<sup>11</sup>. Therefore, in current clinical practice, bone strength is predicted indirectly by evaluating bone mass. However, while measurement of bone mineral density (BMD) is effective for understanding the general status of bone, it is ill-suited to microscopic evaluation of localized characteristics<sup>12</sup>.

Nakano *et al.* have focused on biological apatite (BAP) crystallite alignment within the bone as a more precise method of detecting localized changes at the nano-microscale<sup>13</sup>. BAP crystallite alignment is an important factor in bone quality, which also encompasses other parameters, including bone microstructure, metabolic

turnover, presence of microfractures, and degree of calcification<sup>14</sup>. The orientation of BAP crystals is known to play a role in the mechanical function of bone<sup>15-17</sup>. Furthermore, the c-axis orientation of BAP crystals shows a marked response to local stress. Therefore, clarifying its characteristics would help determine the intensity and direction of mechanical stress<sup>18</sup>.

The hindlimb-unloaded mouse is an outstanding model for directly altering and evaluating bone mechanical function<sup>19</sup>. By suspending the mouse tail so that only the forelimbs are in contact with the ground, functional pressure on the hindlimbs is removed, resulting in decreased hindlimb bone mass. Morey-Holton *et al.* reported that the animal is able to walk freely using the forelimbs, thereby minimizing stress and other systemic influences and allowing clarification of localized bone changes due to mechanical unloading<sup>20</sup>. Peres-Ueno *et al.* investigated femoral BMD in hindlimb-unloaded mice and discussed the increased risk of bone fracture associated with decreased BMD<sup>21</sup>. Furthermore, hindlimb-unloading in rats decreases BMD, leading to decreased bone formation and increased bone resorption<sup>20</sup>. Disuse atrophy after bone fracture, and jaw bone resorption associated with tooth loss are classic examples of structural changes in human bone associated with unloading<sup>22,23</sup>. Thus, studies regarding the effects on bone of removing mechanical stress by tail suspension in mice have provided many useful suggestions in medicine, dentistry, and pharmacy. However, the majority of these reports focused mainly on bone mass and many points remain to be clarified regarding variations in bone mechanical function

reflecting the local load environment. The aim of study was to clarify some of the effects of unloading on qualitative parameters of bone tissue by evaluating changes in the femoral micro- and nanostructures of hindlimb-unloaded mice.

## MATERIALS AND METHODS

### Specimens

Specimens were obtained from 12-week-old male C57BL6 mice ( $n=8$ ) housed under a 12-h light/dark cycle with ad libitum access to food and water. Animal care and maintenance and experimental handling were approved by the Ethics Committee of Tokyo Dental College (Ethics Application No. 290102). After one week of acclimatization, mice were randomly allocated to a conventionally reared (control) group ( $n=4$ ) or a hindlimb-unloaded group ( $n=4$ ). Tails of mice in the hindlimb-unloaded group were sterilized and wrapped in a double layer of elastic and non-elastic tape, to which a wire with a pre-attached clip was fixed (Fig. 1)<sup>24</sup>. After confirming normal blood circulation to the tail, the tip of the tail wire was attached to a rod on the roof of the cage *via* a swivel and adjusted so that only the forelimbs contacted the floor. Each group was housed in a separate cage for 3 weeks, after which all mice were euthanized with intraperitoneal pentobarbital (200 mg/kg). Bilateral femurs were harvested and fixed in 10% neutral buffered formalin. After ethanol dehydration, specimens were embedded in autopolymerizing epoxy resin (SCANDIPLEX, SCANDIA, Hagen, Germany).

### Measurement sites

Each femur specimen was divided into 10 equal segments perpendicular to the longitudinal axis of the bone and the five segments closest to and including the midpoint of the femur were used for measurements. Labeled 'a' to 'e' starting from the proximal end of the femur (Fig. 2)<sup>25</sup>, the five segments were sectioned using a saw microtome with a 300- $\mu\text{m}$  blade (SP1600, Leica, Wetzlar, Germany), and sanded to a thickness of 150  $\mu\text{m}$  using wet/dry sandpaper of increasing grit (#400, #800, and #1200). The cortical bone of each segment was divided into eight equal regions and measurements were performed at the central point of each region (I–VIII, Fig. 2).

### BMD

In order to measure BMD, specimens were examined by micro-computed tomography (micro-CT, HMX225 Actis4, Tesco, Tokyo, Japan) under the following imaging conditions: tube voltage, 140 kV; tube current, 145  $\mu\text{A}$ ; matrix size, 512 $\times$ 512; magnification,  $\times$ 2.5; slice width, 50  $\mu\text{m}$ ; and slice pitch, 50  $\mu\text{m}$ . Regions of interest (ROI) were established to match the measurement sites. Epoxy resin phantoms ( $\phi$ 6 $\times$ 1 mm) containing hydroxyapatite were used. Phantom densities were as follows: 1,550, 800, 700, 600, 500, 400, 300, and 200  $\text{mg}/\text{cm}^3$ . Based on the calibration curve created by micro-CT imaging of the phantoms, the BMD of points I–VIII were calculated for each specimen using TRI/3D-BON-BMD-PNTM2

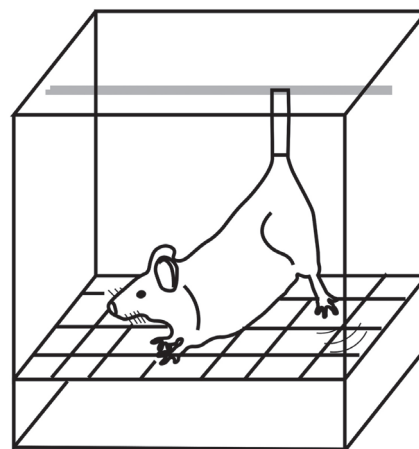


Fig. 1 Overview of hindlimb-unloaded mouse model. An experimental model in which the mouse is suspended by the tail so that only the forelimbs are in contact with the ground; hindlimb unloading causes loss of femoral and tibial bone mass. As the animal is able to walk freely using the forelimbs, stress and other systemic influences are minimized, allowing observation of localized bone changes due to removal of mechanical load.

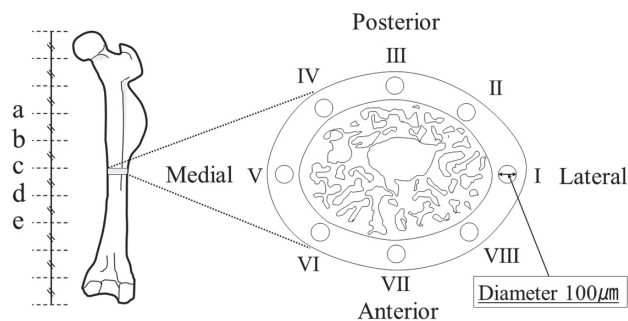


Fig. 2 Establishing measurement sites and points. The entire mouse femur was divided into 10 equal segments perpendicular to the longitudinal axis of the bone and the five segments closest to the midpoint of the femur were used for measurements. These five segments were labeled 'a' to 'e' starting from the proximal end of the femur. The cortical bone of each segment was divided into eight equal regions and measurements were performed at the central points, labeled I–VIII. The diameter of the incident beam during X-ray diffraction analysis was 100  $\mu\text{m}$ .

software (RATOC System Engineering, Tokyo, Japan).

### BAP crystallite alignment

Quantitative analysis of BAP crystallite alignment was conducted using an optical curved imaging plate (IP) X-ray diffraction system (XRD; D/MAX RAPID  $\alpha$ -CMF, Rigaku, Tokyo, Japan). Measurements were performed in reflection and transmission modes with Cu-K $\alpha$  as the

radiation source at a tube voltage of 40 kV and tube current of 30 mA. Reference axes were established in the anteroposterior (X-axis), mediolateral (Y-axis), and longitudinal (Z-axis) directions for each sample (Fig. 3). The line connecting the most upper point of the greater trochanter and the lowest point of the femur is taken as the Z axis<sup>26)</sup>. The radiation site was determined using the XRD's light microscope (magnification, ×0.6–4.8) and an incident beam with a diameter of 100 μm was applied, centered on the midpoint of the cortical bone.

The diffracted X-ray beam was detected as a diffraction ring on the IP. Using transmission mode in the X- and Y-axis directions, and reflection mode in the Z-axis direction, the diffracted X-ray beam was detected using a curved IP based on the conditions described by Nakano *et al.*<sup>27)</sup>. The diffracted X-ray beam was detected as a diffraction ring on the IP. Using 2D Data Processing software (Rigaku), X-ray diffraction intensity ratios were

calculated for the two diffraction peaks corresponding to planes 002 and 310.

Measurements were performed three times at each point (I–VIII) and the mean X-ray diffraction intensity ratio was calculated.

*Statistical analysis*

Two way analysis of variance (ANOVA) was performed regarding BMD and BAp crystallite alignment with comparison between the control and hindlimb-unloaded groups as factor A and differences between segments a–e as factor B. Factors for which a significant difference was observed were tested using *t* test and Tukey's multiple comparison test. Significance was set at *p*<0.05.

RESULTS

*BMD*

BMD at each measurement point is shown in Table 1. BMD for each segment (a–e) was evaluated using mean values for measurement points I–VIII (Fig. 4). Significant differences were observed between the

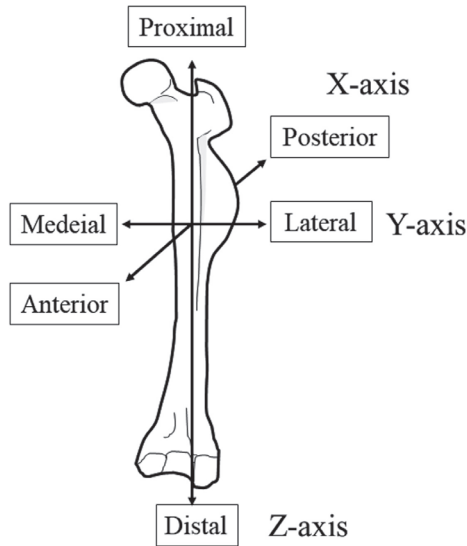


Fig. 3 Establishing the direction of reference axes. Reference axes were established in the mediolateral (X-axis), anteroposterior (Y-axis), and longitudinal (Z-axis) directions.

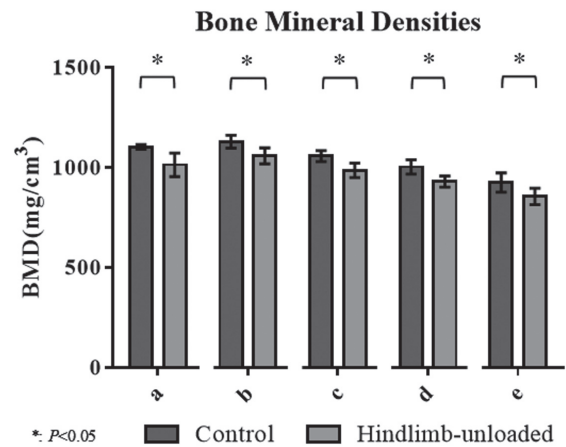


Fig. 4 BMD in each segment (a–e). BMD were lower in the hindlimb group compared to the control group in all segments (*n*=8; *t* test and Tukey's multiple comparison test).

Table 1 BMD (mg/cm<sup>3</sup>) at points I–VIII in segments a–e

	Control group (mg/cm <sup>3</sup> )								Hindlimb-unloaded group (mg/cm <sup>3</sup> )							
	I	II	III	IV	V	VI	VII	VIII	I	II	III	IV	V	VI	VII	VIII
a	1,094.9	1,113.8	1,094.3	1,087.1	1,111.9	1,113.4	1,100.4	1,175.6	996.8	1,128.4	982.7	1,003.4	1,001.4	964.6	987.5	974.2
b	1,161.3	1,072.4	1,159.1	1,134.9	1,131.1	1,120.5	1,149.6	1,111.6	1,056.4	1,104.7	1,052.3	1,026.1	1,114.8	1,006.5	1,049.3	1,045.5
c	1,073.5	1,005.0	1,075.5	1,073.7	1,050.2	1,063.0	1,073.2	1,134.7	981.8	1,017.7	960.6	977.4	1,037.8	939.9	950.4	972.4
d	1,044.8	950.3	1,031.0	974.9	997.3	1,020.9	1,021.4	1,078.4	914.2	964.1	901.7	943.3	953.9	899.3	935.3	924.9
e	974.5	887.1	968.5	858.8	902.5	957.5	954.0	1,005.1	863.7	911.5	812.5	858.3	885.6	804.8	868.5	910.3

BMD for each segment (a–e) was evaluated using mean values for measurement points I–VIII. Significant differences were observed between the control and hindlimb-unloaded groups in all segments.

Table 2 Two-way analysis of variance regarding BMD for factors A and B

Factor	Sum of squares	Degrees of freedom	Mean square	F-value	p-value	Determination
Factor A	130,258	1	130,258	112.6	$p < 0.01$	—
Factor B	370,967	4	92,742	80.16	$p < 0.01$	—
Interaction	1,888	4	472	0.41	$p = 0.81$	—
Error	80,986	70	1,157	—	—	—
Overall	584,099	79	—	—	—	—

Significant differences in BMD were observed on two-way ANOVA for both factors A and B.

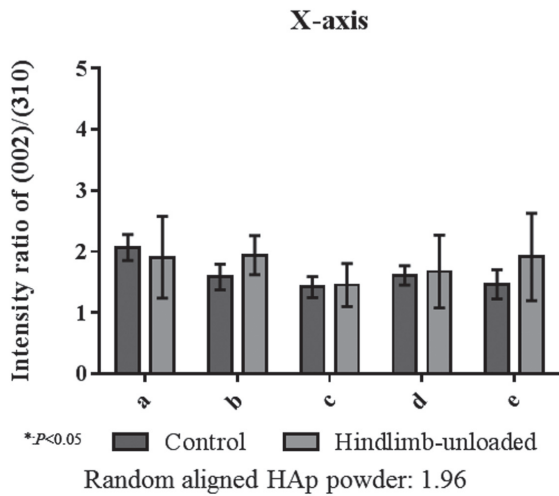


Fig. 5 X-ray diffraction intensity ratios in the X-axis (mediolateral) direction. No significant difference in BAp crystallite alignment was observed in the X-axis direction for factor A ( $n=8$ ; Two way ANOVA,  $t$  test and Tukey's multiple comparison test).

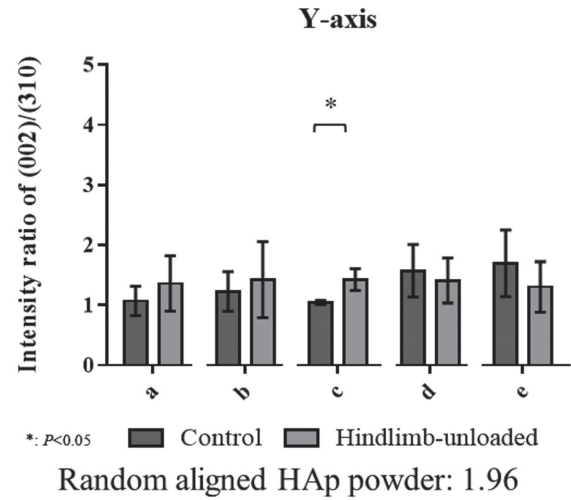


Fig. 6 X-ray diffraction intensity ratios in the Y-axis (anteroposterior) direction. Significant changes in BAp crystallite alignment were observed in segment c (central diaphyseal segment). ( $n=8$ ; Two way ANOVA,  $t$  test and Tukey's multiple comparison test).

Table 3 X-ray diffraction intensity ratios in the Z-axis direction at points I–VIII in segments a–e

		I	II	III	IV	V	VI	VII	VIII
a	Control	2.87	2.72	3.03	2.72	4.36	3.31	3.49	3.09
	HUL	3.05	2.55	2.63	2.38	4.19	2.73	3.27	2.83
b	Control	4.38	3.25	3.47	3.11	3.62	3.15	2.85	3.37
	HUL	2.15	2.54	2.76	2.41	3.08	2.45	3.19	3.26
c	Control	4.83	4.22	3.51	3.59	3.21	3.34	3.16	3.17
	HUL	2.99	2.40	2.39	2.42	3.00	2.69	2.54	3.44
d	Control	2.80	2.09	1.92	1.99	3.44	2.96	2.99	3.38
	HUL	3.13	2.97	2.88	2.61	4.19	3.57	3.22	2.99
e	Control	3.11	2.60	2.76	2.84	4.12	3.80	3.28	3.54
	HUL	3.43	2.44	2.13	2.79	2.61	3.42	2.98	3.53

Random aligned HAp powder: 1.02

Control group: Control

Hindlimb-unloaded group: HUL

Significant differences were also observed between points I, II, and IV in segments b and c for factor A.

\*:  $p < 0.05$  (Factor A)

control and hindlimb-unloaded groups in all segments. Table 2 shows the result of the two-way ANOVA. The results show that significant differences in BMD were observed for both factors A and B. However as a result of the multiple comparison test, no site-based differences were observed.

#### BAP crystallite alignment

The X-ray diffraction intensity ratios on the X-axis for each region (a–e) were evaluated using the mean values for measurement points I–VIII (Fig. 5). No significant differences were observed between control and hindlimb-unloaded groups. The X-ray diffraction intensity ratios on the Y-axis for each region (a–e) were evaluated using the mean values for measurement points I–VIII (Fig. 6). No significant differences were observed between control and hindlimb-unloaded groups except for segment c. However, both the ratio for the control and hindlimb-unloaded groups were lower than non-aligned hydroxyapatite (HAP; 1.96). The X-ray diffraction intensity ratios on the Z-axis at each measurement point are shown in Table 3. The X-ray diffraction intensity ratios on the Z-axis for each region (a–e) were evaluated using the mean values for measurement points I–VIII (Fig. 7). In segment a–c, significantly lower intensity ratios (indicating a low degree of BAP crystallite alignment) were noted in hindlimb-unloaded group.

No significant differences in BAP crystallite alignment were observed on two-way ANOVA in the X-axis (Table 4) or Y-axis (Table 5) directions for either

factor A or B. However, a highly significant difference was observed in the Z-axis direction for factor A ( $p < 0.05$ ).

No significant differences were observed in

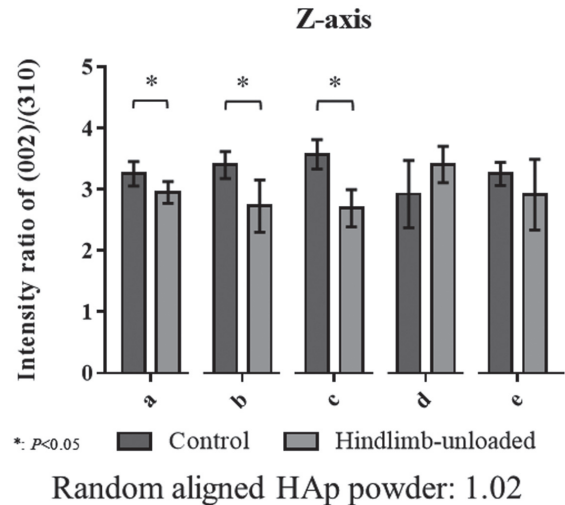


Fig. 7 X-ray diffraction intensity ratios in the Z-axis (longitudinal) direction.

A significant difference in BAP crystallite alignment was observed in the Z-axis direction for factor A. Furthermore, significant changes in BAP crystallite alignment were observed in segments a, b, and c ( $n=8$ ; Two way ANOVA,  $t$  test and Tukey's multiple comparison test).

Table 4 Two-way analysis of variance regarding BAP crystallite alignment in the X-axis direction for factors A and B

Factor	Sum of squares	Degrees of freedom	Mean square	F-value	$p$ -value	Determination
Factor A	0.44	1	0.43	1.40	$p=0.24$	—
Factor B	2.52	4	0.63	2.02	$p=0.11$	—
Interaction	0.98	4	0.25	0.79	$p=0.54$	—
Error	21.80	70	0.31	—	—	—
Overall	25.74	79	—	—	—	—

No significant differences in BAP crystallite alignment were observed on two-way ANOVA in the X-axis directions for either factor A or B.

Table 5 Two-way analysis of variance regarding BAP crystallite alignment in the Y-axis direction for factors A and B

Factor	Sum of squares	Degrees of freedom	Mean square	F-value	$p$ -value	Determination
Factor A	0.08	1	0.08	0.26	$p=0.26$	—
Factor B	1.20	4	0.30	1.03	$p=0.40$	—
Interaction	1.71	4	0.43	1.48	$p=0.22$	—
Error	20.19	70	0.29	—	—	—
Overall	23.17	79	—	—	—	—

No significant differences in BAP crystallite alignment were observed on two-way ANOVA in the Y-axis directions for either factor A or B.

Table 6 Two-way analysis of variance regarding BAp crystallite alignment in the Z-axis direction for factors A and B

Factor	Sum of squares	Degrees of freedom	Mean square	F-value	p-value	Determination
Factor A	2.29	1	2.29	8.49	$p=0.00$	**
Factor B	0.38	4	0.10	0.35	$p=0.84$	—
Interaction	4.71	4	1.18	4.36	$p=0.00$	**
Error	18.90	70	0.27	—	—	—
Overall	26.29	79	—	—	—	—

Significant differences in BAp crystallite alignment were observed on two-way ANOVA in the Z-axis directions for factor A.

X-ray diffraction intensity ratios based on diffraction performed in transmission mode in the X-axis direction. Furthermore, X-ray diffraction intensity ratios in both the control and hindlimb-unloaded groups were lower than the ratio for non-aligned hydroxyapatite (HAp; 1.96).

Significant differences were observed in X-ray diffraction intensity ratios based on diffraction performed in transmission mode in the Y-axis direction for factor A in the central diaphyseal segment (segment c).

However, X-ray diffraction intensity ratios in the Y-axis direction in both the control and hindlimb-unloaded groups were lower than the ratio for non-aligned hydroxyapatite (HAp; 1.96).

Significant differences were observed in X-ray diffraction intensity ratios based on diffraction performed in reflection mode in the Z-axis direction for factor A in segments a, b, and c ( $p<0.05$ ).

X-ray diffraction intensity ratios in the Z-axis direction in both the control and hindlimb-unloaded groups were higher than the ratio for non-aligned hydroxyapatite (HAp; 1.02), demonstrating preferential alignment of BAp crystallites. Significant differences were also observed between points I, II, and IV in segments b and c for factor A ( $p<0.05$ , Table 6).

## DISCUSSION

### BMD

BMD was significantly lower in the hindlimb-unloaded group than in the control group; however, no regional differences in BMD observed. These findings are consistent with those of a previous study investigating the effects of weightlessness on bone mass<sup>28</sup>). While studies such as those by Peres-Ueno and by Aguirre have investigated various bone parameters including BMD in hindlimb-unloaded mice, there have been few reports on regional BMD differences<sup>21,29</sup>).

### BAp crystallite alignment

The present study found uniaxial preferential alignment of BAp crystallites in the longitudinal (Z-axis) direction in all regions of the femoral diaphysis. These findings are consistent with those of Nakano *et al.* demonstrating BAp crystallite c-axis alignment along the longitudinal

axis of the long bones in rabbits<sup>27</sup>). The absence of BAp crystallite alignment in the X- and Y-axis directions can be attributed to optimization of the long bones such as the femur to the load environment. Meanwhile, uniaxial preferential alignment along the longitudinal axis of the bone was still minimally retained even in the hindlimb-unloaded group. The direction of BAp alignment was maintained, despite significantly lower X-ray diffraction intensity ratios in the longitudinal axis direction in the hindlimb-unloaded group when compared to the control group. These findings suggest that bone quality plays a major role in maintaining the mechanical environment, which was maintained despite removal of the weight of the bone itself and exercise load by tail suspension. Slight differences in bone quality depending on the region of the femoral diaphysis were identified, with localized differences in susceptibility to the effects of hindlimb unloading. Specifically, greater decreases in alignment in the Z-axis direction with hindlimb unloading were observed in the Lateral compared to the Medial regions in segments b and c, while little localized difference was observed in segments a, d, and e. The result of this study suggested that the BAp crystallite alignment as a tendon attachment was affected by the functional pressure of the muscle as Bacon *et al.* have reported<sup>30</sup>).

Classic examples of structural changes in human bone associated with unloading are disuse atrophy after bone fracture, and jaw bone resorption associated with tooth loss<sup>31,32</sup>). Furuya *et al.* reported preferential alignment in the direction of loading; specifically, in the direction of masticatory force in the alveolar area in the anterior region of the human dentate jaw<sup>33</sup>). Conversely, Furukawa *et al.* reported decreased mechanical stress associated with tooth loss and resorption of alveolar bone resulting in changes in jaw bone quality to resemble that of the long bones<sup>34</sup>). While the mandible is suspended by the masticatory muscles and is thus little affected by gravity, it is conversely specialized for absorbing functional pressures such as occlusal force<sup>35,36</sup>). Therefore, although tooth loss causes a gradual change in structure to resemble that of long bone; the structural characteristics of the edentulous mandible differ greatly from those of other long bones, which are affected by gravity, and much remains to be clarified. In the unloaded femur, the micro- and nanostructural characteristics,

as well as the macrostructure, resemble those found in the mandible with alveolar bone resorption. Due to the removal of gravity and exercise load from the femur, hindlimb-unloaded mice could provide a model of the edentulous mandible.

## CONCLUSION

Removal of load on femur by hindlimb-unloading in rats was found to cause a reduction in bony substance, in addition to the decrease in bone mass that has already been reported. At the same time, the external contours of the bone remained unchanged and there were no changes in the normal trends in structural properties of the rat femur, indicating a single-axis preferential orientation along the longitudinal axis of the bone. These results suggest that the reduction in the functional pressure needed to maintain homeostasis leads to decreases in both bone mass and bone substance, but the minimum bone structural properties needed to retain the external contours of the bone are conserved.

## ACKNOWLEDGMENTS

The present study was partly supported by research aid from the Private University Research Branding Project from MEXT of Japan (2018) and Grants-in-Aid for Scientific Research (Basic Research (C): 17K11808 and Basic Research (C): 18K09643). We would like to thank Prof. Masao YOSHINARI, Drs. Masaaki KASAHARA, Kei KITAMURA, Takehiro FURUKAWA, and Eiko WATANABE for their technical assistance.

## CONFLICTS OF INTEREST

The authors declare that there are no conflicts of interest.

## REFERENCES

- 1) Oppl B, Michitsch G, Misof B, Kudlacek S, Donis J, Klaushofer K, *et al.* Low bone mineral density and fragility fractures in permanent vegetative state patients. *J Bone Miner Res* 2014; 29: 1096-1100.
- 2) Lang T, Leblanc A, Evans H, Lu Y, Genant H, Yu A. Cortical and trabecular bone mineral loss from the spine and hip in long-duration spaceflight. *J Bone Miner Res* 2004; 19: 1006-1012.
- 3) Berg HE, Eiken O, Miklavcic L, Mekjavic IB. Hip, thigh and calf muscle atrophy and bone loss after 5-week bedrest inactivity. *Eur J Appl Physiol* 2007; 99: 283-289.
- 4) Leblanc AD, Schneider VS, Evans HJ, Engelbretson DA, Krebs JM. Bone mineral loss and recovery after 17 weeks of bed rest. *J Bone Miner Res* 1990; 5: 843-850.
- 5) Rittweger J, Beller G, Armbrrecht G, Mulder E, Buehring B, Gast U, *et al.* Prevention of bone loss during 56 days of strict bed rest by side-alternating resistive vibration exercise. *Bone* 2010; 46: 137-147.
- 6) Yang P, Jia B, Ding C, Wang Z, Qian A, Shang P. Whole-body vibration effects on bone before and after hind-limb unloading in rats. *Aviat Space Environ Med* 2009; 80: 88-93.
- 7) Frost HM. Bone's mechanostat: a 2003 update. *Anat Rec A Discov Mol Cell Evol Biol* 2003; 275: 1081-1101.
- 8) Rodan GA. Bone mass homeostasis and bisphosphonate action. *Bone* 1997; 20: 1-4.
- 9) Tyrovolas JB. The "Mechanostat Theory" of Frost and the OPG/RANKL/RANK system. *J Cell Biochem* 2015; 116: 2724-2729.
- 10) Ireland A, Ferretti JL, Rittweger J. Imaging of the muscle-bone relationship. *Curr Osteoporos Rep* 2014; 12: 486-495.
- 11) Al Nazer R, Lanovaz J, Kawalilak C, Johnston JD, Kontulainen S. Direct in vivo strain measurements in human bone —a systematic literature review. *J Biomech* 2012; 45: 27-40.
- 12) Dougherty G. Quantitative CT in the measurement of bone quantity and bone quality for assessing osteoporosis. *Med Eng Phys* 1996; 18: 557-568.
- 13) Nakano T, Kaibara K, Ishimoto T, Tabata Y, Umakoshi Y. Biological apatite (BAP) crystallographic orientation and texture as a new index for assessing the microstructure and function of bone regenerated by tissue engineering. *Bone* 2012; 51: 741-747.
- 14) NIH consensus development panel on osteoporosis prevention, diagnosis, and therapy. *Osteoporosis prevention, diagnosis, and therapy. JAMA* 2001; 285: 785-795.
- 15) Elliot JC. Structure and chemistry of the apatites and other calcium orthophosphates. Elsevier Sci Amsterdam 1994; 18: 1-389.
- 16) Daculsi G, Bouler JM, LeGeros RZ. Adaptive crystal formation in normal and pathological calcifications in synthetic calcium phosphate and related biomaterials. *Int Rev Cytol* 1997; 172: 129-191.
- 17) Sasaki N, Matsushima N, Ikawa T, Yamaura H, Fukuda A. Orientation of bone mineral and its role in the anisotropic mechanical properties of bone-transverse anisotropy. *J Biomech* 1989; 22: 157-164.
- 18) Nakano T, Ishimoto T, Umakoshi Y, Tabata Y. Texture of biological apatite crystallites and the related mechanical function in regenerated and pathological hard tissues. *J Hard Tissue Biol* 2005; 14: 363-364.
- 19) Hefferan TE, Evans GL, Lotinun S, Zhang M, Morey-Holton E, Turner RT. Effect of gender on bone turnover in adult rats during simulated weightlessness. *J Appl Physiol* 2003; 95: 1775-1780.
- 20) Morey-Holton ER, Globus RK. Hindlimb unloading of growing rats: a model for predicting skeletal changes during space flight. *Bone* 1998; 22: 83-88.
- 21) Peres-Ueno MJ, Stringhetta-Garcia CT, Castoldi RC, Ozaki GAT, Chaves-Neto AH, Dornelles RCM, *et al.* Model of hindlimb unloading in adult female rats: Characterizing bone physicochemical, microstructural, and biomechanical properties. *PLoS One* 2017; 12: e0189121.
- 22) Rittweger J, Winwood K, Seynnes O, de Boer M, Wilks D, Lea R, *et al.* Bone loss from the human distal tibia epiphysis during 24 days of unilateral lower limb suspension. *J Physiol* 2006; 577: 331-337.
- 23) Tallgren A. The effect of denture wearing on facial morphology: A 7-year longitudinal study. *Acta Odontol Scand* 1967; 25: 563-592.
- 24) Morey-Holton ER, Globus RK. Hindlimb unloading rodent model: technical aspects. *J Appl Physiol* (1985) 2002; 92 : 1367-1377.
- 25) Abe S, Watanabe H, Hirayama A, Shibuya E, Hashimoto M, Ide Y. Morphological study of the femur in osteopetrotic (op/op) mice using microcomputed tomography. *Br J Radiol* 2000; 874: 1078-1082.
- 26) Martin RB, Atkinson PJ. Age and sex-related changes in the structure and strength of the human femoral shaft. *J Biomech* 1977; 10: 223-231.
- 27) Nakano T, Kaibara K, Tabata Y, Nagata N, Enomoto S, Marukawa E, *et al.* Unique alignment and texture of biological apatite crystallites in typical calcified tissues analyzed by

- microbeam X-ray diffractometer system. *Bone* 2002; 31: 479-487.
- 28) Wang J, Ishimoto T, Nakano T. Unloading-induced degradation of the anisotropic arrangement of collagen/apatite in rat femurs. *Calcif Tissue Int* 2017; 100: 87-94.
- 29) Aguirre JI, Plotkin LI, Stewart SA, Weinstein RS, Parfitt AM, Manolagas SC, *et al.* Osteocyte apoptosis is induced by weightlessness in mice and precedes osteoclast recruitment and bone loss. *J Bone Miner Res* 2006; 21: 605-615.
- 30) Bacon GE, Bacon PJ, Griffiths RK. Orientation of apatite crystals in relation to muscle attachment in the mandible. *J Biomech* 1980; 13: 725-729.
- 31) Jonasson G, Skoglund I, Rythén M. The rise and fall of the alveolar process: Dependency of teeth and metabolic aspects. *Arch Oral Biol* 2018; 96: 195-200.
- 32) Hackney KJ, Ploutz-Snyder LL. Unilateral lower limb suspension: integrative physiological knowledge from the past 20 years (1991-2011). *Eur J Appl Physiol* 2012; 112: 9-22.
- 33) Furuya H, Matsunaga S, Tamatsu Y, Nakano T, Yoshinari M, Ide Y, *et al.* Analysis of biological apatite crystal orientation in anterior cortical bone of human mandible using microbeam X-ray diffractometry. *Mater Trans* 2012; 53: 980-984.
- 34) Furukawa T, Matsunaga S, Morioka T, Nakano T, Abe S, Yoshinari M, *et al.* Study on bone quality in the human mandible—Alignment of biological apatite crystallites. *J Biomed Mater Res B Appl Biomater* 2019; 107: 838-846.
- 35) de Jong WC, Korfage JA, Langenbach GE. The role of masticatory muscles in the continuous loading of the mandible. *J Ant* 2011; 218: 625-636.
- 36) Gröning F, Fagan M, O'higgins P. Comparing the distribution of strains with the distribution of bone tissue in a human mandible: a finite element study. *Anat Rec* 2013; 296: 9-18.